Variational Image Registration with Local Properties

Sven Kabus[1,2], Astrid Franz[2], and Bernd Fischer[1]

[1] Institute of Mathematics, University of Lübeck, 23560 Lübeck, Germany
[2] Philips Research Laboratories, 22335 Hamburg, Germany
sven.kabus@philips.com

Abstract. In this paper we are concerned with elastic medical image registration. By spatially varying parameters, a displacement field can be reached which is adapted to local material properties. In addition, it enables the introduction of discontinuities within the displacement field inbetween different anatomical structures, like bones and soft tissue. The capability of this approach is demonstrated by various academic examples.

1 Introduction

Nonrigid image registration is a challenging field of growing importance in medical imaging. The task is to find a vector field of displacements such that each point in a template image can be mapped onto a corresponding point in a reference image in a 'meaningful' manner.

By the notion 'meaningful' often a type of constraint is meant which both preserves the topology and prescribes identical elastic properties throughout the image domain. However, there exist several cases where changes in topology are essential and/or where anatomical structures behave different from each other. For instance, structures which are connected in one image may be disconnected in the other image, like the brain-skull interface subject to a brain shift. Furthermore, structures may move along each other and thereby causing discontinuities, like the liver or a joint and their surrounding tissues. In addition, soft tissue is of different elasticity compared to bone structures and therefore behaves different. Also, preservation of shape or volume may be a reasonable property.

Typically, the wanted displacement is computed subject to a smoothness constraint. For example, the constraint is realized by a regularization based on the linear elastic potential of the displacement. In general, the constraint is applied globally with one global regularization parameter and – for the elastic regularizer – with elastic properties independent from the image position. Usually, such a method provides satisfactory results due to the underlying physical model. Nonetheless it fails in cases described above, since a global regularization does not allow for any local changes in topology or material properties. Therefore, in this note a 'meaningful' transformation enables changes in topology, supports local material properties, possibly approximates a shape or volume preservation

J.P.W. Pluim, B. Likar, and F.A. Gerritsen (Eds.): WBIR 2006, LNCS 4057, pp. 92–100, 2006.

and requires, to this end, a locally varying regularization. As a consequence, further a priori knowledge has to be added. This can be achieved by a segmentation of the template image only.

In the literature one can find several attempts dealing with nonrigid image registration in conjunction with spatially varying regularization or material parameters, for example the radial basis functions [1], the Bezier tensor product [2], the B-spline with subsequent filtering [3], the damped springs [4], the finite elements [5, 6, 7] or the finite differences [8] based approaches, respectively. However, these methods either do not reflect the physical behavior of the underlying material, or the registration yields a smooth transformation field, allowing for no discontinuities at all.

In [9, 10] we briefly introduced a new approach which overcomes the above mentioned shortcomings. In this note we extend the new idea and describe the method in greater detail. The following section is concerned with its mathematical formulation whereas Section 3 addresses the numerical treatment. Finally, we demonstrate its advantages by application to academic examples.

2 Variational Approach

Let $R, T : \Omega \to G$ denote the reference and the template image, respectively. Here, G denotes a set of gray values and $\Omega \subset \mathbb{R}^d$ the d-dimensional image region. In addition, let a meaningful segmentation of T be given. That is, a decomposition of Ω into disjoint regions Ω_l is assumed, such that $\Omega = \cup_{l=0}^{m} \Omega_l$. For convenience, let Ω_0 denote the background of image T.

The registration aims at finding a displacement field $\boldsymbol{u} : \Omega \to \mathbb{R}^d$ such that $T_{\boldsymbol{u}} := T(\boldsymbol{id} + \boldsymbol{u})$ is similar to R, where $\boldsymbol{id}$ denotes the identity mapping. In mathematical terms, the similarity is described by a functional $\mathcal{D}[\boldsymbol{u}; T, R]$. $\mathcal{D}$ can be chosen as any popular distance (or similarity) measure provided its Gâteaux derivative exists. However, this note is restricted to the common sum of squared differences, $\mathcal{D}[\boldsymbol{u}; T, R] = \int_\Omega [R(\boldsymbol{x}) - T_{\boldsymbol{u}}(\boldsymbol{x})]^2 \mathrm{d}\boldsymbol{x} =: \int_\Omega L^{\mathcal{D}} \mathrm{d}\boldsymbol{x}$, which assumes monomodal images.

A registration based on a similarity measure only, may yield a deformed template image which perfectly matches the reference image as long as all gray values are present in both images. However, the problem is ill-posed and the underlying deformation does in general not make sense in a physical context. Therefore, an additional smoothness constraint (or regularizer) is considered which can be chosen to model the application specific physical properties. Also, it may be interpreted as a penalizer. In this note we investigate a regularizer based on the popular linear elastic potential which is in addition equipped with spatially varying parameters (the so-called *variable elastic regularizer*),

$$\mathcal{S}[\boldsymbol{u}; \alpha, \lambda, \mu] = \int_\Omega \alpha_{\boldsymbol{u}} \left(\frac{\mu_{\boldsymbol{u}}}{4} \sum_{i,j=1}^{d} (\partial_{x_j} u_i + \partial_{x_i} u_j)^2 + \frac{\lambda_{\boldsymbol{u}}}{2} (\nabla \cdot \boldsymbol{u})^2 \right) \mathrm{d}\boldsymbol{x} =: \int_\Omega L^{\mathcal{S}} \mathrm{d}\boldsymbol{x},$$

where $\alpha_{\boldsymbol{u}}$, $\lambda_{\boldsymbol{u}}$ and $\mu_{\boldsymbol{u}}$ are defined in analogy with $T_{\boldsymbol{u}}$. For other regularizers including diffusive-, fluidal- or curvature-based approaches we refer to, e.g., [11].

In contrast to a conventional approach, where α, λ and μ are global constants, all the three parameters are assumed to be spatially dependent. Here, the positive weighting function $\alpha : \Omega \to \mathbb{R}^+$ describes the local influence of the regularizer. By knowing the segmentation of the template image we are now in a position to reduce the regularization of the displacement field locally and, therefore, to allow for local changes in the topology. To this end, $\alpha \ll 1$ is set in the background region Ω_0, cf. [10]. The Lamé parameters $\lambda, \mu : \Omega \to \mathbb{R}^+$ are used to reflect the material properties. From a qualitative point of view, μ is inversely proportional to the elastic modulus and λ/μ is proportional to the incompressibility of the material. For a detailed interpretation and a comparison of values for specific anatomical structures used in the literature we refer to [7]. Again, by exploiting the segmentation of T, different elastic properties can be assigned to each subdomain Ω_l. Thereby diverse elastic behavior of different materials, like bones and muscles, can be simulated.

Note, that $\alpha_{\boldsymbol{u}}$, $\lambda_{\boldsymbol{u}}$ and $\mu_{\boldsymbol{u}}$ depend on the displacement $\boldsymbol{u}$. This dependency is indispensable due to the fact that nonlinear registration approaches mostly employ an iterative scheme and therefore the material properties at a fixed position do change in the course of the registration. As a consequence, the parameters at an intermediate stage can be deduced from $\boldsymbol{u}$ applied to the initial setting which makes a segmentation of the reference image redundant.

By combining the similarity measure and the regularizing term, the problem is to find a displacement field $\boldsymbol{u}$ which minimizes the joint functional

$$\mathcal{J}[\boldsymbol{u}] := \mathcal{D}[\boldsymbol{u}] + \mathcal{S}[\boldsymbol{u}] = \int_\Omega L^{\mathcal{D}} \mathrm{d}\boldsymbol{x} + \int_\Omega L^{\mathcal{S}} \mathrm{d}\boldsymbol{x}. \tag{1}$$

The computation of the Gâteaux derivative of (1) yields a necessary condition for $\boldsymbol{u}^*$ being a minimizer of (1),

$$\nabla_{\boldsymbol{u}} L^{\mathcal{D}} + \nabla_{\boldsymbol{u}} L^{\mathcal{S}} - \nabla_{\nabla \boldsymbol{u}} L^{\mathcal{S}} = \boldsymbol{0}.$$

Here, $\nabla_{\boldsymbol{u}}$ refers to the gradient with respect to $(u_1, \ldots, u_d)$ whereas $\nabla_{\nabla \boldsymbol{u}}$ denotes the gradient with respect to the Jacobian of $\boldsymbol{u}$. The outcome is a system of nonlinear partial differential equations equipped with associated boundary conditions,

$$\begin{aligned} \mathcal{A}\boldsymbol{u} + \boldsymbol{g}(\boldsymbol{u}) + \boldsymbol{f}(\boldsymbol{u}) &= \boldsymbol{0} \qquad \text{on } \Omega, \\ \frac{\partial u_i}{\partial \boldsymbol{n}} &= 0 \qquad \text{on } \partial\Omega,\ i = 1, \ldots, d, \end{aligned} \tag{2}$$

where $\boldsymbol{f}(\boldsymbol{u}) := -(R - T_{\boldsymbol{u}})\nabla T_{\boldsymbol{u}}$ results from differentiating the similarity measure and is therefore independent from the choice of a regularizer. For the variable elastic regularizer a straightforward calculation yields

$$\begin{aligned} \mathcal{A}\boldsymbol{u} &:= -\nabla \cdot [\alpha_{\boldsymbol{u}} \mu_{\boldsymbol{u}} (\nabla \boldsymbol{u} + \nabla^{\mathsf{T}} \boldsymbol{u})] - \nabla[\alpha_{\boldsymbol{u}} \lambda_{\boldsymbol{u}} \nabla \cdot \boldsymbol{u}] \quad \text{and} \\ \boldsymbol{g}(\boldsymbol{u}) &:= \frac{1}{4} \sum_{i,j=1}^{d} (\partial_{x_j} u_i + \partial_{x_i} u_j)^2 \nabla[\alpha_{\boldsymbol{u}} \mu_{\boldsymbol{u}}] + \frac{1}{2} (\nabla \cdot \boldsymbol{u})^2 \nabla[\alpha_{\boldsymbol{u}} \lambda_{\boldsymbol{u}}]. \end{aligned} \tag{3}$$

Here, we collected terms with a linear dependency on $\boldsymbol{u}$ or on its derivatives in $\mathcal{A}\boldsymbol{u}$ and those with a nonlinear dependency in $\boldsymbol{g}(\boldsymbol{u})$. This allocation will become handy in the numerical treatment. Note that $\mathcal{A}\boldsymbol{u} = \boldsymbol{g}(\boldsymbol{u}) + \boldsymbol{f}(\boldsymbol{u})$ corresponds to the Navier-Lamé equations. The boundary conditions in (2) are of Neumann type but clearly they may be chosen problem dependent.

3 Numerical Treatment

By introducing an artificial time variable, (2) can be linearized as

$$(\boldsymbol{id} + \tau\mathcal{A})\boldsymbol{u}^{(k+1)} = \boldsymbol{u}^{(k)} - \tau\boldsymbol{f}(\boldsymbol{u}^{(k)}) - \tau\boldsymbol{g}(\boldsymbol{u}^{(k)}), \tag{4}$$

where $\boldsymbol{u}^{(k+1)} := \boldsymbol{u}(\boldsymbol{x}, t_{k+1}) = \boldsymbol{u}(\boldsymbol{x}, t_k + \tau)$ and $\boldsymbol{u}^{(0)} \equiv \boldsymbol{0}$. Due to the allocation into $\mathcal{A}$ and $\boldsymbol{g}$, the differential operator $\boldsymbol{id} + \tau\mathcal{A}$ is linear.

The system of partial differential equations (4) can be discretized on a staggered grid using second order finite differences yielding a $d \times d$ block matrix. It turned out to be reasonable to discretize (3) without evaluating the divergence operator first. Otherwise the matrix will be non-symmetric for varying parameters. As a consequence, the discretized form of (3) requires the evaluation of α, λ and μ on interlaced grid positions. Whereas λ and μ could be interpolated either on a full- or on a half-integer grid, the definition of α on a half-integer grid is crucial. For example consider two adjacent anatomical structures. A displacement independently chosen for both structures requires a reduced regularity inbetween (i.e. a thin gap of background region). By defining α on the full-integer grid, a separate row (column) would be needed to incorporate the reduced regularity. When coarsening the scale the same row (column) would still be needed becoming more and more dominating compared to the size of the adjacent image structures. In contrast, defining α on a half-integer grid does not increase the dominance of the gap and is therefore recommended for a multiscale approach. However, a minimum gap size of inter-voxel width is required on the finest image level.

For stability reasons, derivatives of $\boldsymbol{g}$ are approximated by the minmod slope technique [12].

The arising system of equations is of size dN (N being the total number of voxels in Ω). This system has to be solved at every iteration step. The system matrix resembles the Navier-Lamé differential operator and includes the additional information given by the segmentation and local parameters. The righthand-side results from both the similarity measure and further derivative terms due to the dependency of the parameters on $\boldsymbol{u}$.

Finally, to evaluate the deformed template image $T_{\boldsymbol{u}}(\boldsymbol{x})$ and to build up the linear system of equations for the following iteration step, interpolation for $\alpha_{\boldsymbol{u}}$, $\lambda_{\boldsymbol{u}}$ and $\mu_{\boldsymbol{u}}$ is required.

From a theoretical point of view the variational approach and its numerical treatment is suitable for any dimension. However, in this note we only report on results for the more instructive 1D and 2D cases. For a practical treatment, multiresolution and multigrid techniques are advisable.

4 Results

The proposed method has been applied to various academic images. Note that in 1D the variable elastic regularizer simplifies to a variable diffusive regularizer, cf. [10].

1D gap example. In order to outline some fundamental properties of the new approach we start with a 1D image consisting of five objects (cf. Fig. 1, top left, for the template image). Each object (given by an interval with non-zero gray values) belongs to a single region Ω_l, $l = 1, \ldots, 5$, which is encoded in the segmented template image by assigning an integer value to each region (center left). For the outer objects there is no change in position during transition from the template image to the reference image (top of second column). The other ones are designed, such that they do change their positions in such a way that gaps between them show up or disappear. From the segmented template image we deduce the values of the weighting function α (bottom left). By setting α small in background regions we expect a displacement function which is constant within each object and inhibits high gradients inbetween.

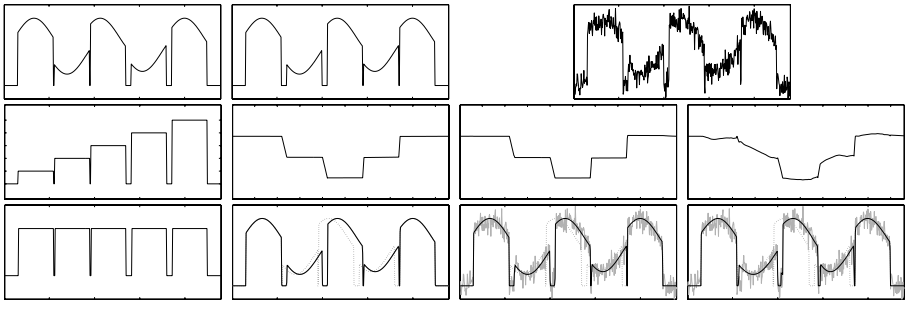

Fig. 1. The template image together with its segmentation and the deduced values for α are shown in the first column (from top to bottom). The second column displays the reference image (top), below the resulting displacement function (center) as well as the transformed template image (bottom), $T_{\boldsymbol{u}}$. In the upper right corner a modified reference image with added 10% white noise is shown. It serves for the results of the third and the fourth column where a varying α and a constant α are chosen, respectively.

As it is apparent from the second column, the variable regularizer applied with $\alpha(x) = 10$ and $\alpha(x) = 0.01$ inside and outside the objects, respectively, nicely fulfills our expectations. The displacement function (center) indicates a constant displacement within the objects with abrupt changes inbetween. Below the transformed template image is depicted. For better comparison we added the (undeformed) template image (dotted line) as well as the reference image (light gray; not visible here due to the coincidence with $T_{\boldsymbol{u}}$). Note that a similar result may be reachable when applying a constant but very small α. However,

this problem is becoming more and more ill-posed the smaller α is and requires, therefore, a smaller step size τ.

To test the proposed method for a more realistic setting, we modified the reference image by adding white noise with a standard deviation of 10% of the previous gray value scale (Fig. 1, top right). The template image and α remain unchanged. The ideal displacement field for this setting remains the same as with the unchanged reference image.

Now, the regularizer has been applied with both a varying (third column) and a constant (fourth column) weighting function. Whereas the constant choice of $\alpha = 0.03$ leads to a dissatisfying result due to the presence of noise in the reference image, a variable weighting (same as for the second column) both supports a noise-independent smooth displacement within the objects and enables for high gradients in the gap regions.

2D rotation example. In the second example we consider the shape-preserving feasibility of the variable elastic regularizer. To this end, a template image with a square is given. A rotation by 30° yields the reference image, cf. Fig. 2. Whereas in the first experiment all parameters are chosen constant, in the second experiment μ is multiplied by 1000 in the square region. Although, after the same number of iterations, both transformed template images almost match the reference image, the varying parameter case (cf. Fig. 2, right) is clearly preferred.

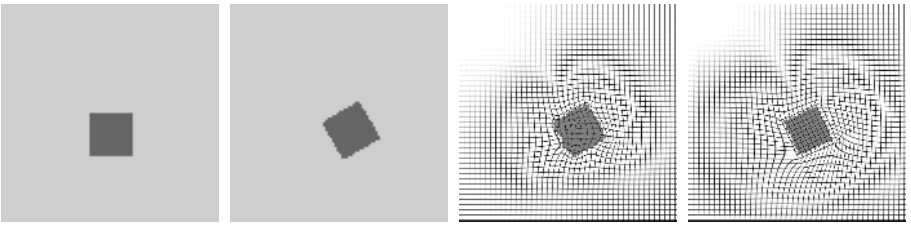

Fig. 2. Template (left) and reference image (center left) are displayed together with visualized displacement fields for a constant μ (center right) and a spatially varying μ (right)

2D phantom image. The last example considers a 2D phantom image (Fig. 3, top left) consisting of three objects: a rectangular object representing, for instance, bone structure, a square object modelling some soft tissue and in its inside a circle object taking the role of, for instance, a tumor. For the transition from the template to the reference image (Fig. 3, top right) we model a shrinking of the tissue object without affecting the bone object, which is usually a problem in registration approaches. The second problem regards the behavior of the circle object. Due to its invisibility in the reference image a conventional registration approach will tend to shrink its size in order to relate it as much as possible to a circle of zero size.

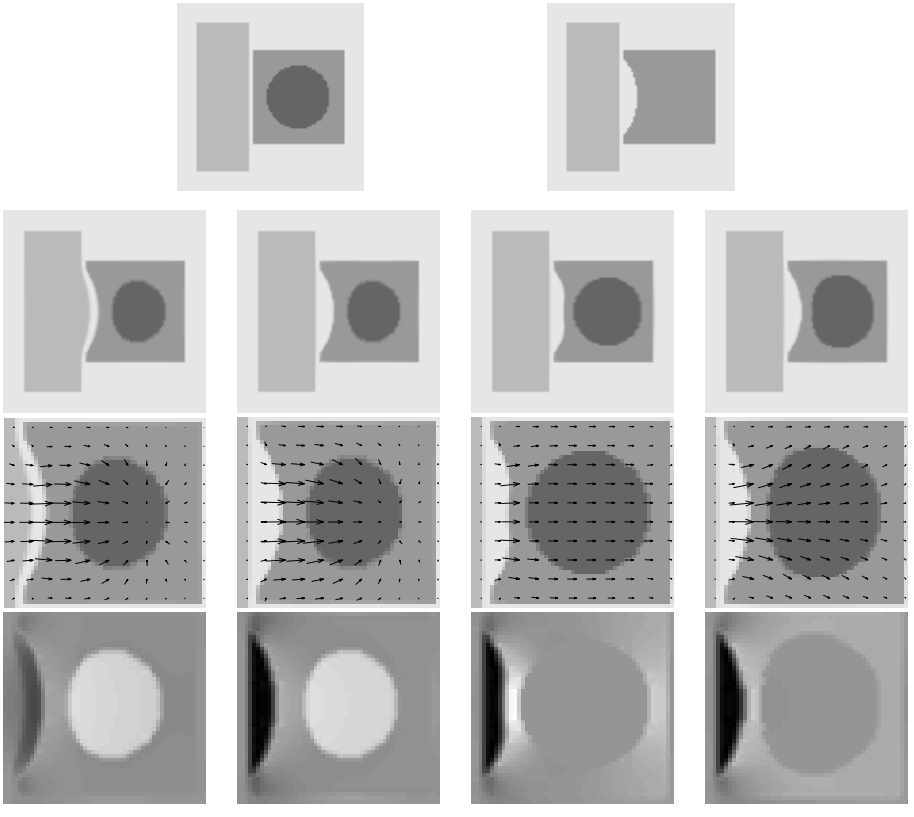

Fig. 3. Below the template and reference image (first row), the results from four different settings are depicted columnwise with respect to $T_{\boldsymbol{u}}$ (second row), the overlayed displacement field (third row; data are thinned out for better recognition) and the volume preservation indicator $|\mathbf{1} + \nabla \boldsymbol{u}|$ (last row), cf. text for further details

The variable elastic regularizer has been employed with four different parameter settings. For the first setting, all parameters are constant ($\alpha \equiv 0.1$, $\lambda \equiv 0.1$, $\mu \equiv 4$), cf. the first column of Fig. 3. For the remaining settings α is reduced locally for all background regions ($\alpha = 0.015$). In addition, for the circle object μ (cf. third column) and λ (cf. fourth column) are multiplied by 1000, respectively.

The resulting deformation fields have been compared with respect to the deformed template image (second row in Fig. 3) and for a zoomed region around the square object with respect to the displacement field (third row) and the quantity $|\mathbf{1} + \nabla \boldsymbol{u}|$ (last row). Here, a volume preserved region (corresponding to $|\mathbf{1} + \nabla \boldsymbol{u}| = 1$) is depicted by medium gray, whereas a contracting (expanding) region appears in light gray (dark gray).

Recalling the first problem, the shrinking of the tissue object without affecting the bone object works properly whenever the weighting of the regularizer is small inbetween (second to fourth column). For the second problem several

observations can be made. With no further material knowledge the tumor object is shrinked (reduction in volume is 30%), indicated by a light gray of the circle object in the bottom row. With a large μ or λ either a shape (and volume) preservation (third column) or an approximated volume preservation only (fourth column) can be seen. For both cases the change in volume is less than 0.3%.

5 Conclusion and Discussion

We have proposed an elastic potential based registration approach with displacement dependent parameters. It has been shown that this approach enables one to incorporate pre-knowledge, for instance the knowledge of anatomical structure or material properties. Whereas a proper choice of the local influence of the regularizer may lead to a discontinuous displacement field in order to model topological changes, different choices for the material parameters allow to mimic different elastic properties. Clearly, exact values for the parameters are not known in general and, usually, are guessed for in vivo situations [7].

Compared to our previous results, now, the segmentation of the template image only is sufficient. This is an important issue for time-critical tasks, like brain-shift, since an (often time-consuming) segmentation is required for the pre-operatively generated image only.

However, as a consequence from skipping the intra-operative segmentation, adjacent anatomical structures require, in order to diverge, a minimum gap of inter-voxel width inbetween. We are currently working on omitting this drawback.

References

1. G.K. Rohde, A. Aldroubi, and B.M. Dawant. The adaptive bases algorithm for intensity-based nonrigid image registration. *IEEE Trans Med Imaging*, 22(11):1470–1479, 2003.
2. G. Soza et al. Non-linear intraoperative correction of brain shift with 1.5 T data. In *Proc. of BVM 2003*, pages 21–25, 2003.
3. M. Staring, S. Klein, and J.P.W. Pluim. Nonrigid registration with adaptive, content-based filtering of the deformation field. In *Proc. of SPIE 2005*, volume 5747, pages 212 – 221, 2005.
4. P.J. Edwards et al. A three-component deformation model for image-guided surgery. *Med Image Anal*, 2(4):355–367, 1998.
5. J. Rexilius et al. Automatic nonrigid registration for tracking brain shift during neurosurgery. In *Proc. of BVM 2002*, pages 135–138, 2002.
6. M. Ferrant et al. Registration of 3D intraoperative MR images of the brain using a finite element biomechanical model. *IEEE Trans Med Imaging*, 20(12):1384–1397, 2001.
7. A. Hagemann. *A Biomechanical Model of the Human Head with Variable Material Properties for Intraoperative Image Correction*. Logos, Berlin, 2001.

8. C. Davatzikos. Nonlinear registration of brain images using deformable models. In *Proc. of the IEEE Workshop on Math. Methods in Biomedical Image Analysis*, pages 94–103, 1996.
9. S. Kabus, A. Franz, and B. Fischer. On elastic image registration with varying material parameters. In *Proc. of BVM 2005*, pages 330–334, 2005.
10. S. Kabus, A. Franz, and B. Fischer. Variational image registration allowing for discontinuities in the displacement field. In *Proc. from the 2005 CMA Conference on Image Processing*, to appear 2006.
11. J. Modersitzki. *Numerical methods for image registration.* Oxford University Press, 2004.
12. R.J. LeVeque. *Numerical Methods for Conservation Laws.* Birkhäuser, 1992.